Contrib Mineral Petrol (2006) 151: 681–697
DOI 10.1007/s00410-006-0087-2

ORIGINAL PAPER

Cliff S. J. Shaw · Florian Heidelbach
Donald B. Dingwell

The origin of reaction textures in mantle peridotite xenoliths from Sal Island, Cape Verde: the case for "metasomatism" by the host lava

Received: 21 November 2005 / Accepted: 16 March 2006 / Published online: 19 April 2006

Abstract Reaction zones around minerals in mantle xenoliths have been reported from many localities worldwide. Interpretations of the origins of these textures fall into two groups: mantle metasomatic reaction or reaction during transport of the xenoliths to the surface. A suite of harzburgitic mantle xenoliths from Sal, Cape Verde show clear evidence of reaction during transport. The reactions resulted in the formation of olivine–clinopyroxene and Si- and alkali-rich glass reaction zones around orthopyroxene and sieve-textured clinopyroxene and sieve textured spinel, both of which are associated with a Si- and alkali-rich glass similar to that in the orthopyroxene reaction zones. Reaction occurred at pressures less than the mantle equilibration pressure and at temperatures close to the liquidus temperature of the host magma. In addition, there is a clear spatial relation of reaction with the host lava: reaction is most intense near the lava/xenolith contact. The residence time of the xenoliths in the host magma, determined from Fe–Mg interdiffusion profiles in olivine, was approximately 4 years. Our results cannot be reconciled with a recent model for the evolution of the mantle below the Cape Verde Archipelago involving mantle metasomatism by kimberlitic melt. We contend that alkali-rich glasses in the Sal xenoliths are not remnants of a kimberlitic melt, but rather they are the result of reaction between the host lava or a similar magma and xenolith minerals, in particular orthopyroxene. The formation of a Si- and alkali-rich glass by host magma–orthopyroxene reaction appears to be a necessary precursor to formation of sieve textured spinel and clinopyroxene.

Communicated by J. Hoefs

C. S. J. Shaw (✉)
Department of Geology, University of New Brunswick,
2 Bailey Drive, Fredericton, NB, Canada E3B 5A3
E-mail: cshaw@unb.ca

F. Heidelbach
Bayerisches Geoinstitut, Universität Bayreuth,
95440 Bayreuth, Germany

D. B. Dingwell
Earth and Environmental Sciences, University of Munich,
80333 Munich, Germany

Introduction

Mantle-derived xenoliths are an essential source of information about the nature and evolution of the lithospheric mantle. These xenoliths are generally assumed to have been transported to the surface rapidly, with little or no alteration of their primary mineralogy. Recent studies (Klügel 1998, 2001a; Shaw 2004; Shaw and Klügel 2002), however, provided the petrologic evidence that xenoliths may reside in crustal magma chambers for significant periods prior to eruption. During such residence periods, xenoliths commonly suffer significant textural modification that may mimic the effects of mantle metasomatism. Clearly, in order to avoid erroneous interpretations of the state of the mantle, its mineralogy and chemical composition, it is of vital importance to be able to identify those textures that are of mantle origin versus those imposed on the xenoliths during magma transport/residence.

A common feature of mantle xenoliths is the occurrence of glass-bearing sieve-textured rims on clinopyroxene and spinel and reaction rims on orthopyroxene (Bonadiman et al. 2005; Carpenter et al. 2002; Coltorti et al. 2000a, b; Pike and Schwarzman 1976; Shaw and Edgar 1997). The origin of these reaction textures and the associated glasses has been the subject of considerable controversy. Carpenter et al. (2002) have suggested that the textural modifications in xenoliths from the Hessian Depression in Germany result from fluid-induced melting in the mantle. Bonadiman et al. (2005) presented an alternative explanation for the origin of sieve-texture in Cape Verde xenoliths; they suggest that the reaction textures

are result of metasomatism induced by the influx of ultrapotassic (kimberlitic) melts into the lithospheric mantle. In contrast, Shaw and Edgar (1997) have interpreted similar textures in xenoliths from Ireland to be the result of magma–xenolith interaction during residence and transport in magma after entrainment. Since these textures are so common in peridotites worldwide, e.g. Canada, Mongolia, SE China, and Mexico (Brearley et al. 1984; Ionov et al. 1994; Liang and Elthon 1990; Qi et al. 1995), it is important that we understand their mode of formation. We need criteria to determine whether they are due to interactions with magma during transport, metasomatic processes in the mantle, or to melting events caused by fluid influx.

Previous studies and rational for this work

In the first study of peridotites from Sal, Cape Verde, de Paepe and Klerkx (1971) recorded the presence of reaction textures but noted that their origin was still uncertain. Ryabchikov et al. (1995) did not note the presence of reaction textures but did describe phlogopite and a variety of glasses ranging from MgO-rich to K_2O-rich. They interpreted these glasses to be relics of melts that were present in the mantle prior to excavation of the xenoliths. Most recently, Bonadiman et al. (2005) have shown that the major and trace element composition of pyroxenes in the Sal xenoliths is consistent with re-equilibration of garnet lherzolites in the spinel facies. They also suggested that the reaction textures in the Sal samples reflect a mantle metasomatic event induced by kimberlite-like melt in the lithospheric mantle.

The goal of this study is to examine this hypothesis for the presence of kimberlitic melt in the Cape Verde lithosphere in light of recent experimental results and detailed studies of zonation profiles in the xenolith minerals. The Cape Verde xenoliths are ideal for this study as they contain fresh glass. Several other studies of textural modification in xenoliths have been hampered by the partial to complete alteration of the glass e.g. Carpenter et al. (2002), Shaw and Edgar (1997).

Sample location and host lava

The samples were collected in December 1997 from the east side of a nephelinitic volcanic plug on the north-end of Sal Island in the Cape Verde archipelago (Fig. 1). A total of seven samples, of the 15 collected, were studied in detail, in most cases two or three sections were produced from each xenolith. The xenoliths range in size from 1 to 7 cm and are sub-rounded to angular. All have a distinct lava crust of clinopyroxene-rich olivine nephelinite that contains both euhedral olivine phenocrysts and subhedral to anhedral olivine xenocrysts. The latter commonly show well-developed deformation features.

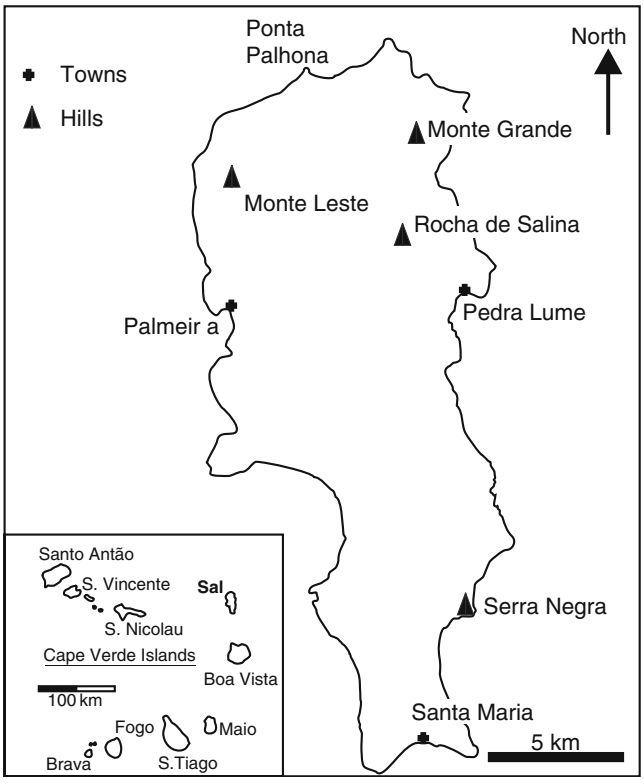

Fig. 1 Sample location on the north end of Sal Island in the Cape Verde Archipelago (after de Paepe and Klerkx 1971)

On the basis of the data published by Doucelance et al. (2003) the host lavas are amongst the most Si-undersaturated in the Cape Verde archipelago with 3–5% total alkalis and a Na_2O/K_2O ratio of 1.7–1.9. The lavas have mg# [molecular $(MgO/(MgO + FeO)) \times 100$] of 74–79 and Ni contents of 466–611 ppm. The mg# is slightly higher than would be expected from a primary magma (BVSP 1981), probably reflecting contamination from mantle-derived olivine.

Petrography of the xenoliths

The xenoliths studied are all harzburgites or orthopyroxene-rich lherzolites (Fig. 2). They comprise olivine grains up to 6 mm in size that have well-developed deformation lamellae and numerous trails of fluid inclusions. Clinopyroxene, orthopyroxene and spinel occur in two textural settings, firstly as inclusions within much larger olivines and secondly as interstitial grains between larger olivine crystals. Olivine is cut by numerous fractures filled with veins of either with light brown glass or black, microlite-rich glass that are clearly connected to the host lava. These veins range in thickness from 20 μm to ~1 mm. Olivine—melt contacts are generally smooth and variably embayed. Embayments vary in depth from a few tens of microns to more than 1 mm. Olivine xenocrysts generally show more embayments than do the olivines at the edge of the xenoliths.

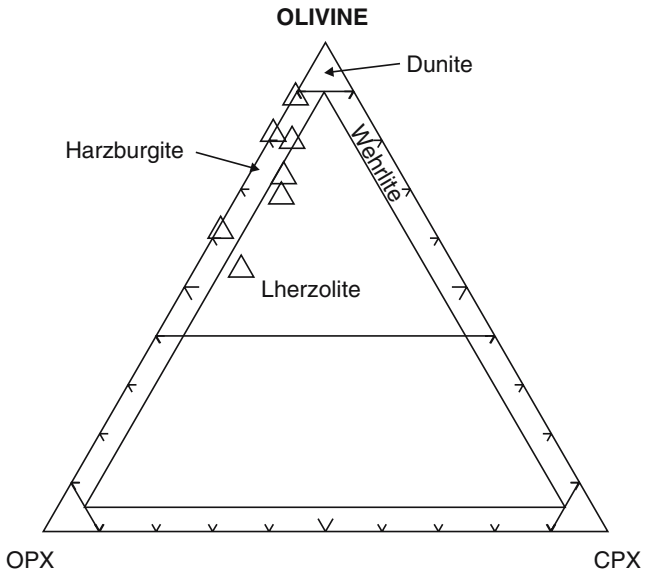

Fig. 2 Classification of the xenoliths based on point count data

Two samples show a distinct association between orthopyroxene and spinel (Fig. 3a). In these zones, thin, elongate, curved spinel grains are intergrown with 1–2 mm orthopyroxene grains. These spinels are distinct from those found elsewhere in the same samples; where there is no association with orthopyroxene, spinel generally forms rounded grains (Fig. 3b). The distribution of orthopyroxene and spinel in these intergrowth zones is suggestive of the former presence of an earlier phase (Fig. 3a) possibly garnet (see Bonadiman et al. 2005), however, Canil (personal communication, 2006) has suggested that they could result from breakdown of an earlier high aluminum orthopyroxene.

Reaction rims

Three distinct types of reaction rim have been identified in the xenoliths and some similar zones have been observed on xenocrysts in the host lava.

Spinel reaction zones

These are 50–300 μm thick zones of opaque spinel surrounding red–brown primary spinel (Fig. 3b). The reaction zones comprise small grains of interconnected secondary black spinel surrounded by glass. The thickness of the reaction zones is variable within any single sample and even in single grains. Sieve-texture occurs on the rims of spinel grains interstitial to olivine or clinopyroxene as well as on spinel in orthopyroxene reaction zones. In all cases, the sieve-textured grains have a variably thick film of melt along their grain boundaries.

Spinel xenocrysts in the host lava have a similar dark rim (Fig. 3c) however, the sieve-texture is less well-developed; there are fewer glass inclusions, and inclusions of groundmass minerals are common.

Clinopyroxene reaction zones

Clinopyroxene typically shows sieve-textured rims (Fig. 3d) particularly near contacts with the host lava, but also within xenoliths. In some cases the complete grain shows sieve texture (Fig. 3e). More typically however, clinopyroxene comprises an inclusion-free core (Fig. 3d) surrounded by a rim of clinopyroxene, olivine, glass and spinel. Clinopyroxene in the rim is in optical continuity with the inclusion-free core, where present, and has numerous vermicular inclusions and embayments filled with glass and in the larger ones olivine and spinel (Fig. 3f).

Orthopyroxene reaction zones

Orthopyroxene reaction zones range in thickness from 100 μm to complete pseudomorphing of grains, up to 3 mm. The thickest reaction zones are found at the contact with the host lava. The reaction zones consist of olivine, glass, clinopyroxene and spinel (Fig. 3g, h) and coexist with reacted clinopyroxene and spinel (Fig. 3b, g). Olivine within the reaction zones is sub- to euhedral and commonly exhibits a long axis perpendicular to the edge of the remaining orthopyroxene. Clinopyroxene is not present in all samples. Where reaction zones are in direct contact with the host lava, however, there are greater amounts clinopyroxene than otherwise, as well as a band of oxides that is not present in internal reaction zones.

Relationship of reaction zones to host lava

In all of the samples examined, the reaction zones, particularly on orthopyroxene and clinopyroxene tend to be thicker on the side of the grain nearest the host lava and much thinner on the "lee" side of the grain (Fig. 4).

Mineral compositions

Analytical methods

Mineral compositions were determined at the University of New Brunswick with a JEOL-733 electron microprobe in wavelength dispersive mode. Minerals were analysed with an accelerating voltage of 15 kV and a current of 10 nA using a 1 μm beam. Glasses were analysed with a defocused, 5 μm beam to reduce Na migration. A variety of natural standards were used for calibration and each element was counted for 30 s on the peak position and 15 s on each background. Raw data were processed using the ZAF correction routine.

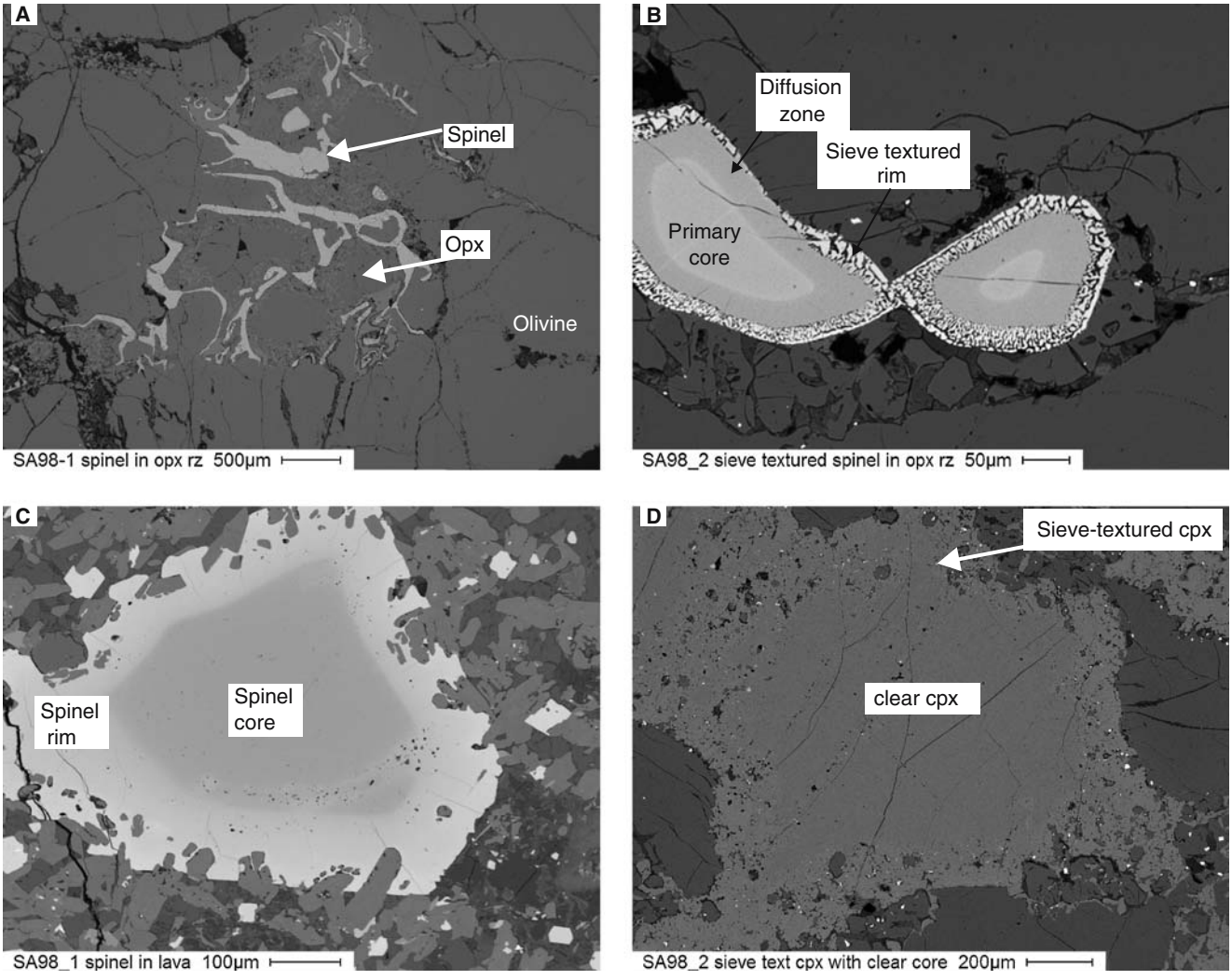

Fig. 3 **a** Intergrowth of elongate spinel and orthopyroxene forming a possible garnet pseudomorph. Note that both the spinel and orthopyroxene show evidence of later reaction. **b** Rounded spinel with a sieve textured reaction zone within the reaction zone around a larger orthopyroxene crystal. **c** Spinel xenocryst in host lava showing a light coloured, inclusion-rich rim. **d** Clinopyroxene with a clear core and a sieve textured rim. **e** Clinopyroxene completely converted to sieve texture with inclusions of olivine and glass. **f** Detail of outlined region from 3e showing the pools of glass and olivine that form the sieve texture in clinopyroxene. **g** One to 2 mm wide reaction zone around a large orthopyroxene crystal showing the typical texture of these zones. **h** Detail of outlined area showing the typical mineral assemblage in an orthopyroxene reaction zone

For compositional traverses though olivine, clinopyroxene and spinel, the microprobe was programmed to step across the sample in increments of 2–10 µm. Based on comparison with a standard, the step size is accurate to within 0.5 µm.

The crystallographic orientation of selected olivine grains was determined by electron backscattering diffraction (EBSD) on sections polished with colloidal silica, to remove material that was damaged during mechanical grinding. The analyses were performed with a LEO Gemini 1530 FEG-SEM at the Bayerisches Geoinstitut. Operating conditions were 20 kV at a working distance of ~20 mm with a beam current of 3.5 nA. Indexing of the diffraction patterns was performed automatically with the CHANNEL software from HKL Technology.

Olivine

Olivine occurs in three distinct textural settings. Primary olivine is coarse-grained and has cores with Fo contents of 87–91, NiO up to 0.35 wt% and CaO <0.2 wt%. Where primary grains are in contact with the host lava, either at the xenolith edge or where veins of the host penetrate the xenoliths, they show distinctive zonation with Fo contents of 79–86 and CaO >0.5 wt% (Table 1).

Secondary olivine in orthopyroxene reaction zones has slightly higher Fo content compared to the cores of primary olivine grains, and is distinctly more magnesian and less calcic than that found on the rims of primary olivine (Table 1).

Olivine in sieve-textured clinopyroxene is indistinguishable from the cores of primary olivine grains.

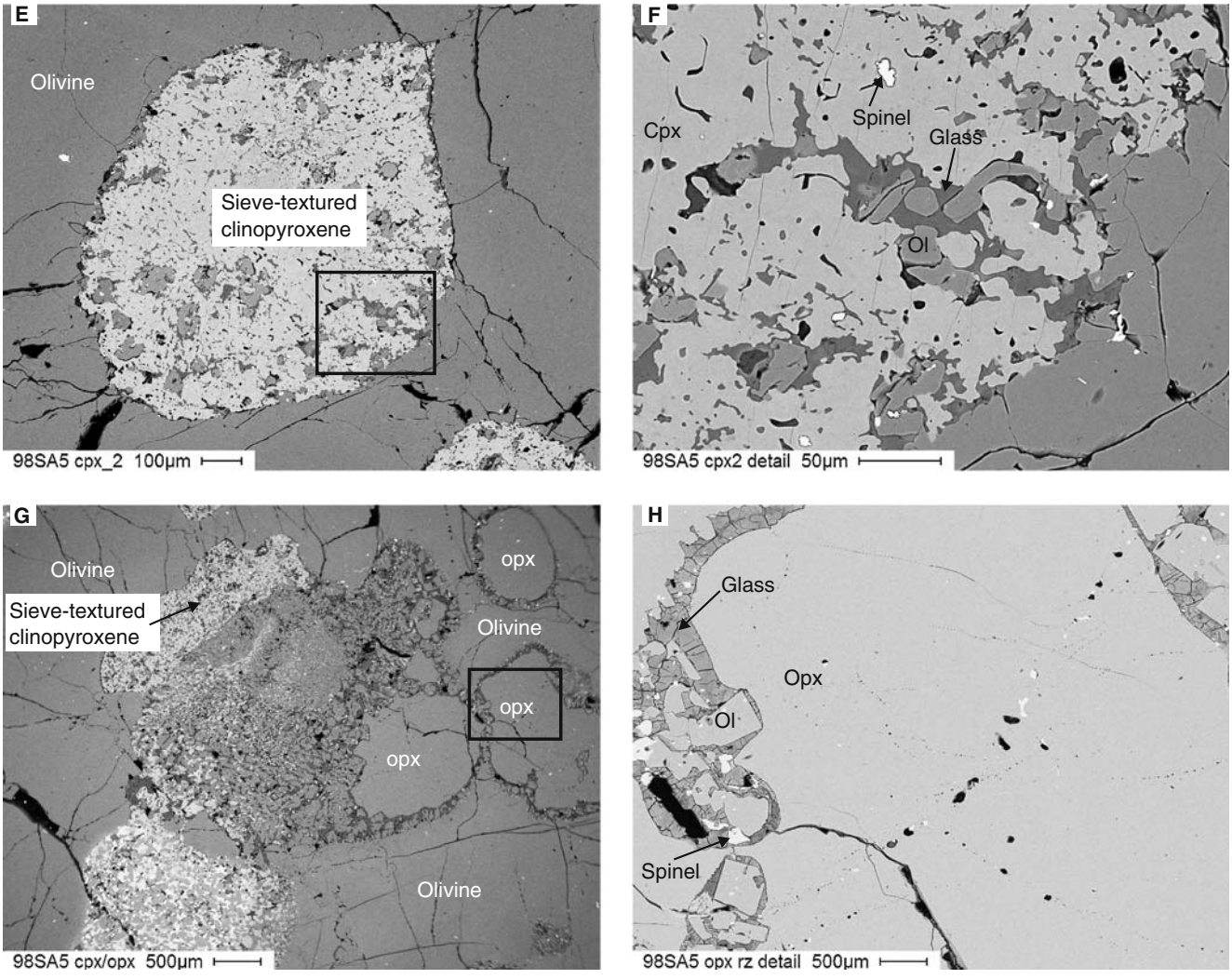

Fig. 3 (Contd.)

Compositional traverses through olivine

Thirty-seven detailed traverses were made through olivine grains in contact with (1) host lava, (2) orthopyroxene reaction zones, (3) sieve-textured clinopyroxene (Fig. 5). The orientation of the traverse relative to the crystallographic axes of the olivine was determined for 15 of the grains.

Olivine in contact with infiltrated glass veins and with orthopyroxene reaction zones shows Fo zonation profiles up to 50 microns wide. Many of these grains also show a distinct increase in CaO toward their rims (Fig. 5a, b).

Olivine in contact with sieve-textured clinopyroxene has a 50–70 μm wide zone in which there is a small decrease in Fo and a distinct increase in the CaO content (Fig. 5c).

Olivine in contact with the host lava, either on the outside of the xenolith or adjacent to 1–2 mm thick veins of host lava shows distinct zonation in Fo and CaO (Fig. 5d–h). The zoned regions range from 100 to 300 μm wide. Three different profiles types have been identified. Type I profiles show a smooth decrease in Fo content from the edge of a plateau in the core of the grain toward the rim (Fig. 5f, g). In most samples the cores have Fo contents of $Fo_{88.5\text{-}91}$ whereas the rims have Fo contents from 81 to 89. On the basis of variation in CaO contents, type I profiles can be divided into two subtypes. Type Ia grains show a smooth increase in CaO from core to rim where CaO contents may be as high as 1.2 wt% (Fig. 5d, f). Type Ib profiles, show distinct humps in the CaO profile that are not reflected or only weakly reflected in the Fo content (Fig. 5e, h). Type II profiles are similar to type I, except that the rim is marked by a plateau in Fo content ranging from 40 to 120 μm thick. CaO in these profiles also shows a plateau at the rim of the grains (Fig. 5g).

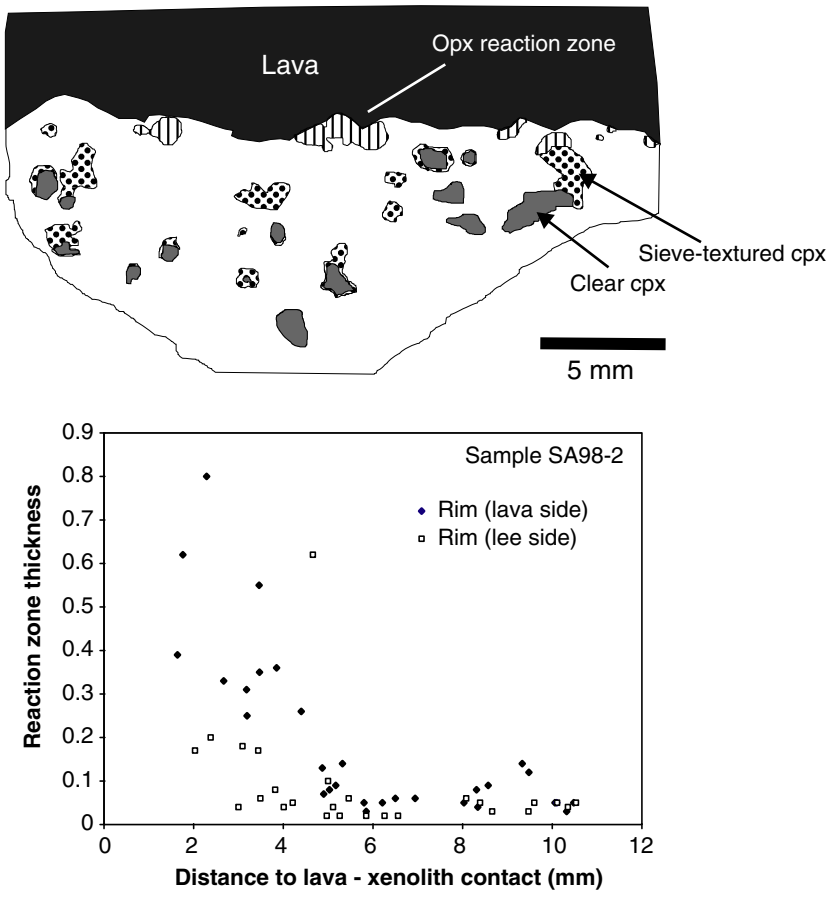

Fig. 4 **a** Sketch of section SA98-5c showing well developed sieve-textured zones in clinopyroxene facing the host lava and poorly developed reaction zones on the lee side. **b** Relationship between reaction zone width and distance to the xenolith contact on orthopyroxene crystals in SA98-2

Several profiles were made in olivine xenocrysts. One of these is similar to the type Ib profiles described above. However, there is also a single xenocryst (Fig. 5i) that has a core of Fo_{80} and a much more magnesian rim (Fo_{84}); this grain also has a low CaO core and high CaO rim.

Clinopyroxene

The inclusion-free cores of primary clinopyroxene are Al–Cr–augite to Al–Cr diopside according to the classification of Morimoto et al. (1988). In common with the

Table 1 Composition of olivine cores and rims

Sample	SA98-5	SA98-5	SA98-4	SA98-4	SA98-4	SA98-4	SA98-3	SA98-3	SA98-2	SA98-2	SA98-1	SA98-1	SA98-3
Location	Core	Rim	Core	Rim	Core	Rim	Core	Rim	Core	Rim	opx rz	opx rz	Incl in cpx
SiO_2	40.11	39.94	40.57	39.26	40.82	39.79	40.69	40.04	40.77	39.14	40.44	40.55	42.19
Al_2O_3	0.06	0.03	0.00	0.03	0.01	0.06	0.04	0.03	0.04	0.05	0.00	0.00	0.00
MgO	47.42	45.82	48.50	41.24	50.26	44.90	49.30	46.55	49.56	42.88	49.98	49.67	49.04
MnO	0.19	0.29	0.10	0.53	0.14	0.35	0.14	0.25	0.08	0.41	0.12	0.14	0.20
FeO	11.68	13.16	10.42	17.65	8.37	13.78	9.18	12.31	8.94	16.13	8.51	8.04	9.67
NiO	0.29	0.17	0.33	0.12	0.38	0.16	0.36	0.27	0.34	0.11	NA	NA	NA
CaO	0.19	0.56	0.06	1.13	0.01	0.95	0.21	0.50	0.20	1.18	0.07	0.11	0.17
Total	99.94	99.97	99.98	99.96	99.98	99.99	99.93	99.94	99.93	99.90	99.12	98.51	101.27
Structural formula based on 4 oxygens													
Si	0.994	0.997	0.998	1.003	0.996	0.997	0.997	0.996	0.997	0.994	0.994	1.001	1.023
Al	0.002	0.001	0.000	0.001	0.000	0.002	0.001	0.001	0.001	0.001	0.000	0.000	0.000
Ni	0.006	0.003	0.007	0.002	0.007	0.003	0.007	0.005	0.007	0.002	0.000	0.000	0.000
Fe	0.242	0.275	0.214	0.377	0.171	0.289	0.188	0.256	0.183	0.343	0.175	0.166	0.020
Mn	0.004	0.006	0.002	0.011	0.003	0.007	0.003	0.005	0.002	0.009	0.003	0.003	0.004
Mg	1.752	1.705	1.779	1.570	1.827	1.678	1.801	1.726	1.807	1.623	1.829	1.827	1.762
Ca	0.005	0.015	0.002	0.031	0.000	0.026	0.006	0.013	0.005	0.032	0.070	0.003	0.004
Fo	87.6	85.5	89.2	79.4	91.4	84.2	90.3	86.5	90.6	81.2	91.0	91.2	89.4
Fa	12.1	13.8	10.7	19.1	8.6	14.5	9.4	12.8	9.2	17.2	8.6	8.2	9.8
Mc	0.3	0.8	0.1	1.6	0.0	1.3	0.3	0.7	0.3	1.6	0.1	0.2	0.4

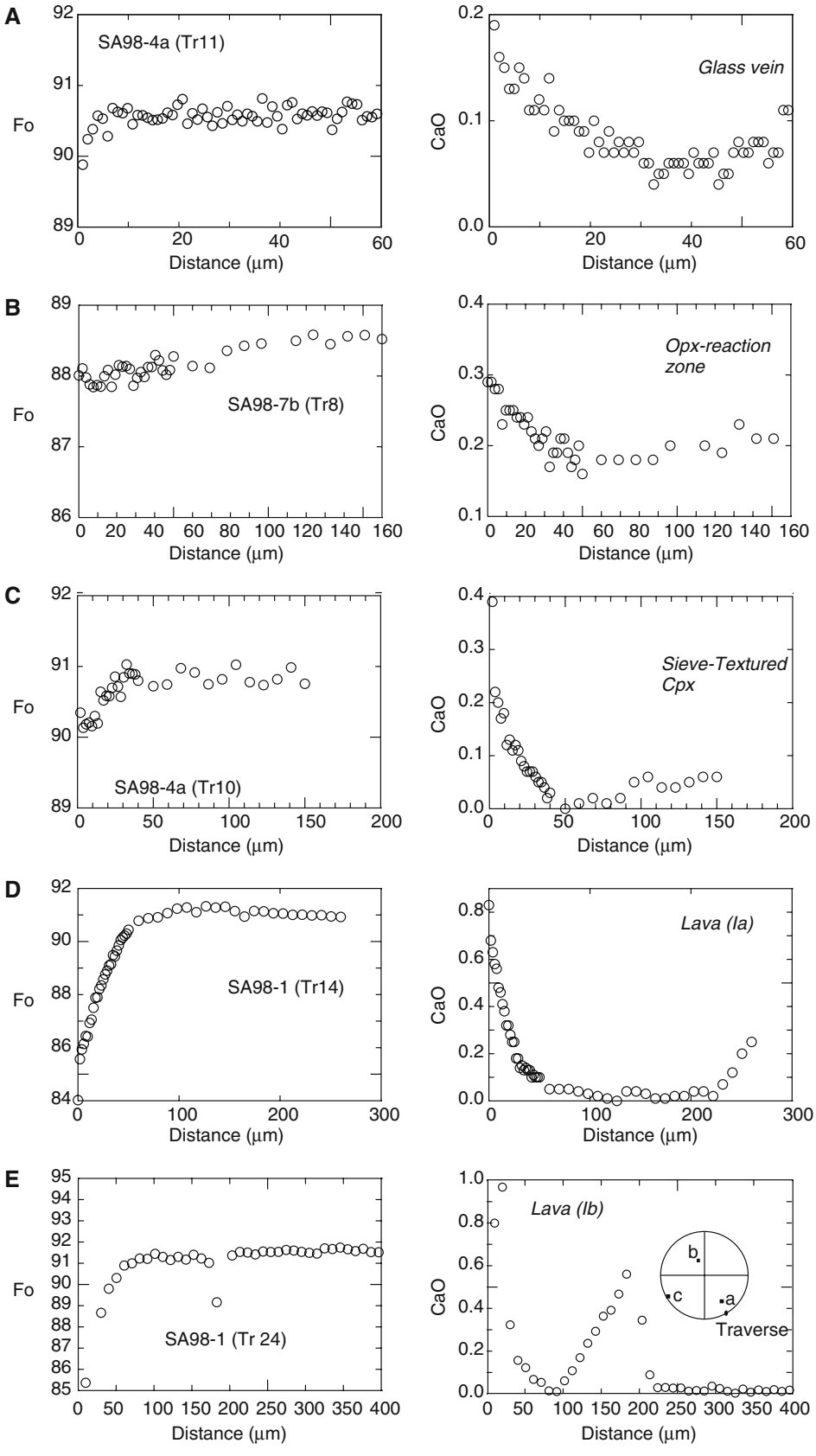

Fig. 5 Compositional traverses in olivine (see text for details)

Fig. 5 (Contd.)

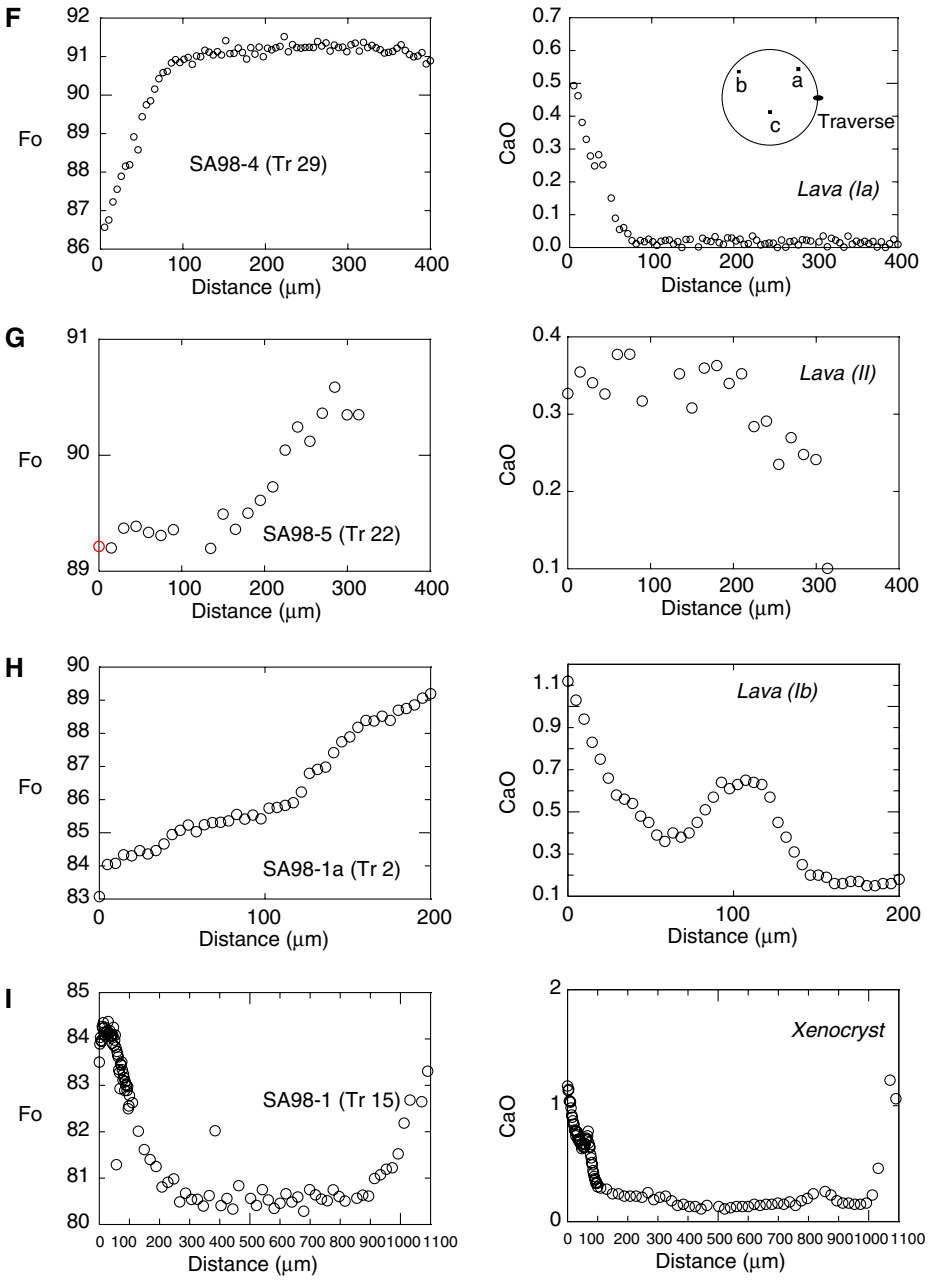

data of Bonadiman et al. (2005) these primary clinopyroxene grains are generally Ca-poor (Table 2).

The sieve-textured clinopyroxene is distinctly less sodic than the cores with higher CaO and lower Al^{vi} (Fig. 6, Table 2). Traverses from the inclusion-free core to the sieve-textured rim of several clinopyroxenes show a consistent pattern of zonation (Fig. 7) with a systematic decrease in Na_2O, Al_2O_3, FeO and MgO from core to rim, coupled with a distinct increase in CaO.

Clinopyroxene phenocrysts in the host lava are titanian Al-rich augite that show normal zonation in terms of mg#.

Orthopyroxene

Orthopyroxene (Table 3) is homogeneous in the samples studied and there is little compositional variation between samples.

Spinel

The cores of sieve-textured spinel grains and cores and rims of spinel with no reaction zones are Ti-poor with high Al_2O_3 and MgO (Table 3). In contrast, spinel in the sieve-textured rims is Ti and Cr-enriched and is depleted in Al_2O_3 and MgO. In common with clinopyroxene and

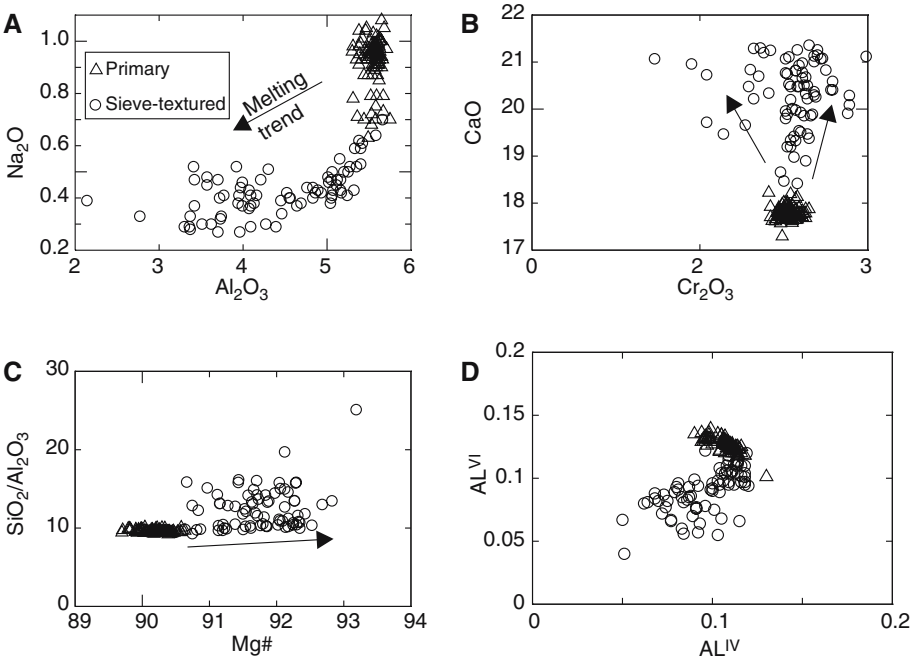

Fig. 6 Composition of clear (primary) cores versus sieve textured rims of clinopyroxene. Note the CaO depleted signature of the cores in (**b**) (cf Bonadiman et al. 2005). The *arrows* show the expected trend of clinopyroxene compositions during melting of peridotite (from Hirose and Kawamoto 1995)

Table 2 Composition of clinopyroxene cores and rims

Sample	SA98-1	SA98-1	SA98-2	SA98-2	SA98-2	SA98-3	SA98-3	SA98-4	SA98-4	SA98-5	SA98-5	SA98-7	SA98-7
Type	Lava	opx rz	Core	Intermed	Rim	Core	Rim	Core	Rim	Core	Rim	Core	Rim
SiO_2	44.82	54.73	52.64	53.71	52.36	52.89	53.51	55.92	55.87	51.58	52.92	53.59	53.21
TiO_2	4.09	0.10	0.14	0.06	0.49	0.07	0.08	0.29	0.15	0.08	0.11	0.11	0.11
Al_2O_3	7.80	0.25	4.90	3.56	3.95	5.41	5.58	0.20	0.15	5.59	3.08	5.38	4.13
Cr_2O_3	0.00	2.12	1.47	0.95	1.86	1.48	1.41	1.23	2.53	1.44	1.33	1.55	1.88
FeO	6.42	2.51	2.92	3.13	2.34	3.60	3.53	2.86	2.60	3.48	2.61	3.52	3.31
MnO	0.04	0.08	0.08	0.09	0.12	0.06	0.04	0.09	0.03	0.09	0.10	0.07	0.05
MgO	12.42	18.87	17.36	17.93	16.26	18.02	18.06	20.06	18.89	17.69	17.42	18.39	18.13
CaO	23.83	18.84	20.62	20.96	22.67	17.49	18.22	19.15	19.27	18.19	21.26	17.65	19.91
Na_2O	0.53	1.03	0.54	0.41	0.55	1.03	0.70	0.80	1.28	0.66	0.32	0.91	0.38
K_2O	0.01	0.00	0.00	0.00	0.01	0.02	0.09	0.03	0.02	0.01	0.04	0.00	0.00
Total	99.95	98.53	100.67	100.81	100.61	100.06	101.22	100.64	100.78	98.80	99.19	101.17	101.11
Mg#	0.78	0.93	0.91	0.91	0.93	0.90	0.90	0.93	0.93	0.90	0.92	0.90	0.91
Structural formula based on 6 oxygens													
Si	1.686	2.002	1.892	1.927	1.895	1.902	1.902	2.000	2.002	1.883	1.932	1.904	1.904
Al(iv)	0.314	0.000	0.108	0.073	0.105	0.098	0.098	0.000	0.000	0.117	0.068	0.096	0.096
Al(vi)	0.031	0.011	0.100	0.078	0.064	0.131	0.136	0.008	0.006	0.123	0.064	0.129	0.078
Ti	0.116	0.003	0.004	0.002	0.013	0.002	0.002	0.008	0.004	0.002	0.003	0.003	0.003
Cr	0.000	0.061	0.042	0.027	0.053	0.042	0.040	0.035	0.072	0.042	0.038	0.044	0.053
Fe	0.202	0.077	0.088	0.094	0.071	0.108	0.105	0.086	0.078	0.106	0.080	0.105	0.099
Mn	0.001	0.002	0.002	0.003	0.004	0.002	0.001	0.003	0.001	0.003	0.003	0.002	0.002
Mg	0.696	1.029	0.930	0.959	0.877	0.966	0.957	1.069	1.009	0.963	0.948	0.974	0.967
Ca	0.960	0.738	0.794	0.806	0.879	0.674	0.694	0.734	0.740	0.711	0.832	0.672	0.763
Na	0.039	0.073	0.038	0.029	0.039	0.072	0.048	0.055	0.089	0.047	0.023	0.063	0.026
Wo	0.517	0.400	0.438	0.434	0.481	0.386	0.395	0.389	0.405	0.399	0.447	0.384	0.417
En	0.375	0.558	0.513	0.516	0.480	0.553	0.545	0.566	0.552	0.541	0.510	0.556	0.529
Fs	0.109	0.042	0.049	0.051	0.039	0.062	0.060	0.046	0.043	0.060	0.043	0.060	0.054

Mg# = MgO/40.4/[(MgO/40.4) + (FeO/71.85)]

olivine there is a distinct compositional variation as shown in Fig. 8. This variation is simple for Ti, and Cr (Fig. 8a, e) however, for Al, Mg and Fe there are distinctive discontinuities in the profiles (Fig. 8b–d, f).

Glass

Silicate glass is found in orthopyroxene reaction zones and in sieve-textured clinopyroxene. Glass may also be

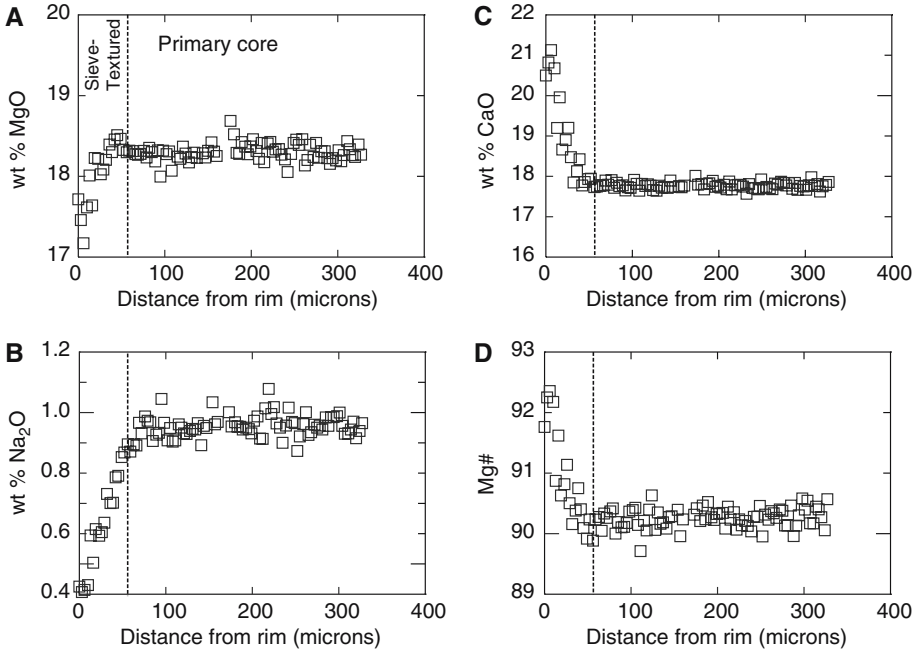

Fig. 7 Compositional traverse in clinopyroxene from SA98-2 showing the difference in composition between the sieve textured zone and the primary clinopyroxene (see text for details)

present in sieve-textured spinel; however, the pockets are too small for reliable analysis.

Glass associated with orthopyroxene

Glass associated with orthopyroxene shows a range of SiO_2 contents from 50 to 65 wt% (Fig. 9, Table 4) and has total alkalis ranging from 3 to 11 wt% (Fig. 9a). Na_2O and K_2O increase sympathetically. $K/(K+Na)$ ratios vary from 0.75 to 0.95 and CaO contents are less than 2 wt%.

Glass associated with clinopyroxene

Glass associated with clinopyroxene is more restricted in SiO_2 content (51–60 wt%) and alkalis (3–9 wt%) and is

Table 3 Composition of orthopyroxene and spinel

Sample	SA98-2 opx	SA98-2 opx	SA98-1 Spinel core	SA98-1 Spinel rim	SA98-2 Spinel core	SA98-2 Spinel rim	SA98-3 Spinel core	SA98-3 Spinel rim	SA98-3 No sieve	SA98-5 Spinel core	SA98-5 Spinel rim	SA98-7 Spinel core	SA98-7 Spinel rim
SiO_2	55.14	54.82	0.02	0.35	0.15	0.52	0.18	0.53	0.16	0.14	0.25	0.19	0.30
TiO_2	0.13	0.01	0.11	0.26	0.12	0.49	0.10	1.25	0.07	0.19	0.75	0.85	0.93
Al_2O_3	4.37	4.83	28.57	13.24	39.62	32.35	38.94	28.70	39.21	42.15	35.08	42.83	45.91
FeO	5.89	5.85	15.34	15.60	13.48	11.85	14.55	16.39	13.73	11.22	12.76	15.50	11.72
MnO	0.12	0.09	0.15	0.32	0.00	0.00	0.00	0.00	0.00	0.15	0.00	0.17	0.12
MgO	32.42	32.03	14.72	11.98	18.98	16.39	18.18	17.45	18.96	17.75	16.35	17.78	17.90
CaO	1.49	1.53	0.01	0.00	0.00	0.02	0.01	0.05	0.00	0.01	0.03	0.00	0.04
Na_2O	0.07	0.11	0.05	0.00	0.01	0.02	0.03	0.02	0.00	0.00	0.00	0.00	0.00
K_2O	0.01	0.00	0.00	0.10	0.00	0.04	0.00	0.01	0.00	0.00	0.00	0.00	0.00
Cr_2O_3	0.97	1.01	40.07	56.48	28.25	39.25	28.36	34.79	28.39	27.18	32.78	22.65	24.00
Total	100.60	100.28	99.04	98.33	100.61	100.92	100.33	99.18	100.53	98.78	97.99	99.97	100.92
Opx formula based on 6 oxygens, spinel formula based on 32 oxygens													
Si	1.897	1.892	0.004	0.092	0.033	0.119	0.040	0.124	0.035	0.031	0.058	0.042	0.065
Al	0.177	0.197	8.055	4.073	10.299	8.766	10.215	7.917	10.214	11.100	9.623	11.135	11.732
Cr	0.026	0.028	7.575	11.651	4.924	7.133	4.989	6.435	4.959	4.800	6.030	3.949	4.113
Fe^{3+a}			0.321	0.000	0.672	0.000	0.682	0.961	0.734	0.000	0.000	0.551	0.000
Ti	0.000	0.000	0.020	0.051	0.020	0.084	0.017	0.220	0.012	0.032	0.130	0.141	0.152
Mg	1.663	1.648	5.246	4.659	6.237	5.616	6.029	6.085	6.243	5.909	5.670	5.843	5.782
Fe^{2+a}	0.170	0.169	2.747	3.413	1.815	2.278	2.025	2.247	1.804	2.122	2.512	2.307	2.125
Mn	0.004	0.003	0.030	0.071	0.000	0.000	0.000	0.000	0.000	0.029	0.000	0.031	0.022
Ca	0.055	0.057	0.001	0.000	0.001	0.004	0.002	0.013	0.000	0.003	0.007	0.001	0.009
Mg#	0.907	0.907	0.631	0.577	0.715	0.711	0.690	0.654	0.711	0.738	0.695	0.671	0.731
Cr#			0.485	0.741	0.324	0.449	0.328	0.448	0.327	0.302	0.385	0.262	0.260

$Cr\# = Cr_2O_3/151.99/[(Cr_2O_3/151.99) + (Al_2O_3/101.96)]$
[a] Fe^{2+} and Fe^{3+} in spinel calculated on basis of stoichiometry

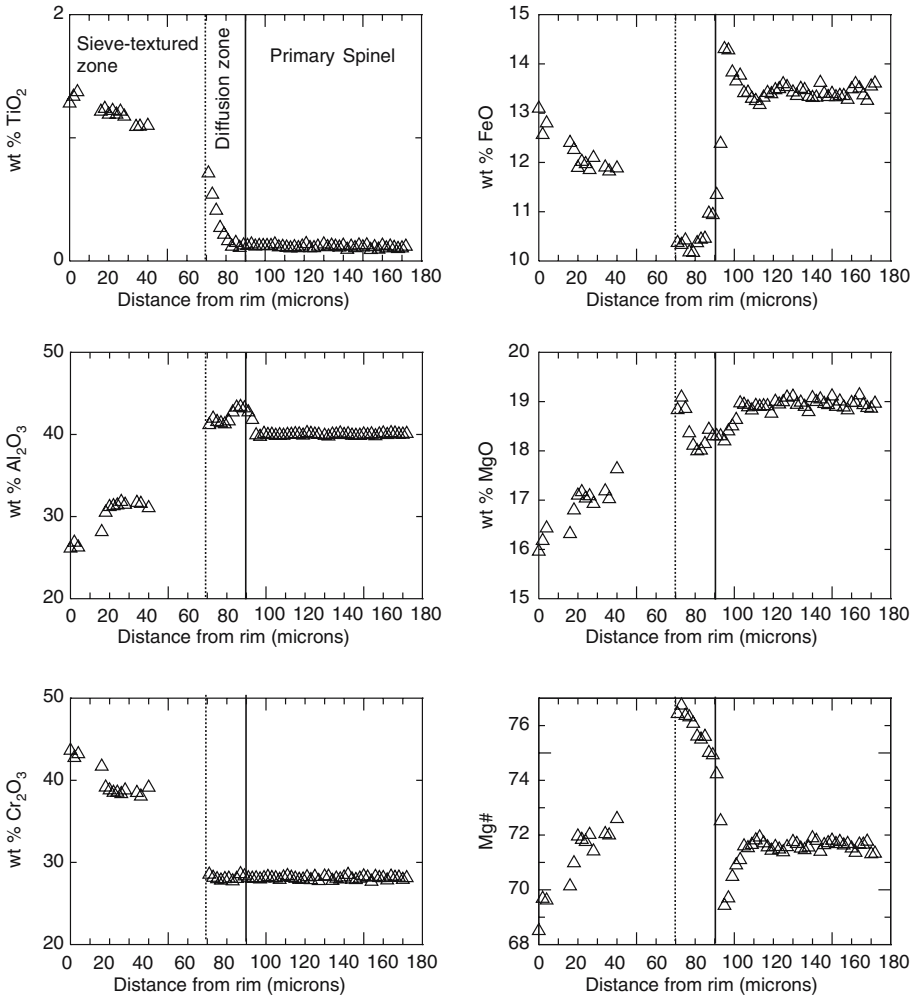

Fig. 8 Compositional traverses in spinel from SA98-2 showing the differences in composition between the sieve-textured reaction zone, diffusion zone and primary spinel core (see text for details)

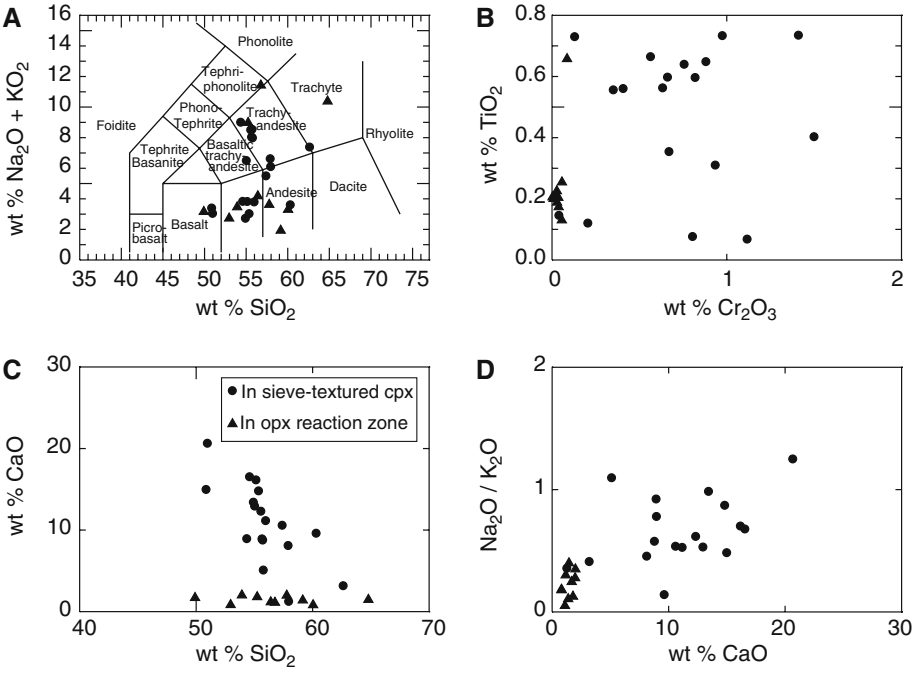

Fig. 9 Composition of glass found in orthopyroxene reaction zones and in sieve textured clinopyroxene

Table 4 Glass compositions

Sample	SA98-3	SA98-3	SA98-3	SA98-3	SA98-3	SA98-3	SA98-3	SA98-3	SA98-3
Associated phase	cpx	cpx	cpx	cpx	cpx	cpx	cpx	cpx	cpx
SiO_2	43.11	50.96	41.93	54.91	50.85	55.02	55.71	57.89	54.34
TiO_2	0.14	0.74	0.39	0.40	0.73	0.64	0.56	0.56	0.56
Al_2O_3	3.90	3.99	6.11	7.07	10.84	12.41	15.56	15.90	16.66
FeO	11.73	2.87	9.29	2.46	2.13	1.87	1.27	2.00	2.18
MnO	0.15	0.05	0.11	0.09	0.04	0.08	0.07	0.03	0.07
MgO	36.74	15.03	31.97	15.40	12.62	8.59	6.14	5.93	6.34
CaO	0.49	20.65	1.39	13.42	14.98	12.94	8.78	8.11	8.95
Na_2O	0.61	1.69	2.64	1.35	1.11	2.26	3.13	2.07	3.95
K_2O	1.62	1.35	3.24	1.37	2.29	4.25	5.42	4.55	5.06
Cr_2O_3	0.09	1.41	0.98	1.50	0.97	0.76	0.41	0.35	0.63
Total	98.58	98.73	98.06	97.98	96.58	98.82	97.06	97.39	98.76
Mg#	0.848	0.903	0.860	0.918	0.913	0.891	0.896	0.840	0.838

	SA98-2	SA98-2	SA98-2	SA98-2	SA98-2	SA98-2	SA98-2	SA98-2	SA98-2
	cpx	cpx	opx	opx	opx	opx	opx	opx	opx
SiO_2	49.01	48.52	51.70	64.79	68.18	68.06	48.52	53.93	57.78
TiO_2	0.10	0.07	0.06	0.66	0.61	0.85	0.07	0.20	0.20
Al_2O_3	9.83	5.01	4.92	16.31	17.13	16.99	5.01	16.30	18.63
FeO	4.99	5.99	2.48	0.59	0.34	0.47	5.99	2.56	1.41
MnO	0.13	0.08	0.06	0.01	0.00	0.00	0.08	0.05	0.30
MgO	30.32	32.52	18.09	2.75	0.36	0.27	32.52	11.52	5.85
CaO	0.51	0.39	13.19	1.45	0.23	0.47	0.39	2.00	1.98
Na_2O	0.92	2.26	1.98	2.95	2.95	2.92	2.26	0.89	0.78
K_2O	2.06	2.75	1.36	7.41	8.21	7.98	2.75	2.56	2.83
Cr_2O_3	0.74	1.40	2.45	0.09	0.01	0.02	1.40	0.01	0.00
Total	98.60	98.97	96.30	97.01	98.02	98.04	98.99	90.02	89.76
Mg#	0.915	0.906	0.929	0.892	0.656	0.500	0.906	0.889	0.881

more sodic, Ti-rich and calcic than glass in orthopyroxene reaction zones (Fig. 9, Table 4). The K/(K + Na) ratio for these glasses ranges from 0.45 to 0.70.

Discussion

Pressure and temperature of equilibration

Ryabchikov et al. (1995) and Bonadiman et al. (2005) provide overlapping estimates of the pressure–temperature conditions under which the Sal xenoliths equilibrated (1.3 and 2.1 GPa; 975 and 1,210°C; based on the geothermobarometers of Brey and Köhler 1990 and Köhler and Brey 1990). The low CaO and HREE contents of the primary clinopyroxene was interpreted by Bonadiman et al. (2005) to indicate that the spinel facies Sal xenoliths originally equilibrated in the garnet facies.

Location of reaction

A major debate in the interpretation of the reaction textures in mantle xenoliths surrounds the question of the location where reaction occurred (see for example Wulff-Pedersen et al. 1999; Klügel 2001b). Simply put, there are two conflicting points of view. Bonadiman et al. (2005); Carpenter et al. (2002) and Ionov et al. (1994) argue for reaction of clinopyroxene, spinel and orthopyroxene in the mantle during a metasomatic episode. The alternative point of view (Brearley et al. 1984; Shaw and Edgar 1997) is that these reaction textures are the result of interactions between the xenoliths and their host magma during or after entrainment. If the latter is true then, although the reactions change the composition and mineralogy of the xenoliths, they are not related to mantle metasomatism sensu stricto and their effects must be removed before interpretations of the history of the lithospheric mantle can be attempted. This is not to say that reactions between melt and the mantle do not occur (c.f. Kelemen et al. 1992). Nevertheless, a major consequence of reaction of orthopyroxene-bearing mantle with silica-undersaturated melts that had infiltrated along grain boundaries would have been complete consumption of orthopyroxene and transformation of the mantle to a wehrlitic assemblage (Shaw et al. 2005). In order to determine the nature and thereby the likely location of the reaction process, three factors must be determined.

(1) Composition of the reacting melt.
(2) Temperature of the reaction.
(3) Pressure of the reaction.

Composition of the reacting melt

Bonadiman et al. (2005) have suggested that the melt responsible for the reactions and the formation of glass in the Sal xenoliths was kimberlitic in composition. They

base this conclusion on linear mixing, mass balance calculations in which they take the starting minerals and products of the reaction and calculate the composition of the metasomatising melt.

On the basis of previous experiments on orthopyroxene—melt reaction (Shaw 1999; Shaw et al. 1998) we contend that this simple model is flawed and leads to calculation of an incorrect melt composition. Shaw (1999) and Shaw et al. (1998) showed that during dissolution of orthopyroxene, there is strong uphill diffusion of K and Na from the silica undersaturated melt into the Si-enriched melt in the reaction zone. This means that a linear mass balance approach to this type of reaction will not yield correct results. To illustrate this point more clearly we have performed mass balance calculations on the orthopyroxene–basanite experiments of Shaw (1999) in which all compositions before and after the experiment are known. The results of these calculations (Fig. 10, Table 5) show that a simple mass balance approach to determining the composition of the reactant melt leads to a large overestimation of the K and Na content and an underestimation of the Ti and Al content. The melt compositions calculated from the experimental data are very similar to those quoted by Bonadiman et al. (2005) for the reacting melt in the Sal xenoliths. These calculations suggest that the glasses associated with reacted minerals in the Sal xenoliths had a silica undersaturated basalt, similar to the host lava, as their parent, rather than the kimberlitic melt suggested by Bonadiman et al. (2005).

Pressure and temperature of reaction

Even though the melt responsible for reaction is similar to the host lava, it remains possible that reaction could have occurred prior to entrainment. Unfortunately there is no geothermobarometer that can be used to determine the pressure of reaction for this scenario. However, Shaw (1999) and Shaw et al. (1998) showed experimentally that the composition of glass in reaction zones on orthopyroxene is pressure dependent, with silica contents exhibiting a marked decrease with increasing reaction pressure. The maximum observed silica contents in the reaction zones range from 65 to 69 wt% at 1 atmosphere thorugh 60–62 wt% at 0.4 GPa, 56–59 wt% at 1 GPa to 44–48 wt% at 2 GPa. All the glass analysed in this study and in the study of Bonadiman et al. (2005) is silica-rich (60–68 wt%). Comparison of these glasses with experimental data suggests that the Sal glasses formed at relatively low pressures, probably between atmospheric pressure and 1 GPa, but certainly less that 2 GPa. Given that the available equilibration data for the xenoliths indicates a higher-pressure mantle source, we propose that the reaction zones and their associated glasses are not a result of melt infiltration and metasomatism in the mantle. Rather they result from interactions between the xenoliths and their host magma during their passage from the mantle to the surface.

The temperature of reaction was estimated using the MELTS program (Ghiorso and Sack 1995) to match the composition of olivine rims in the xenoliths with the equilibrium composition of the liquidus olivine in the lava. This yields an approximate reaction temperature of 1,175°C.

Textural evidence for a relationship between reaction zones and the host lava

Evidence for a causal relationship between the reaction zones and the host lava is perhaps best illustrated by the

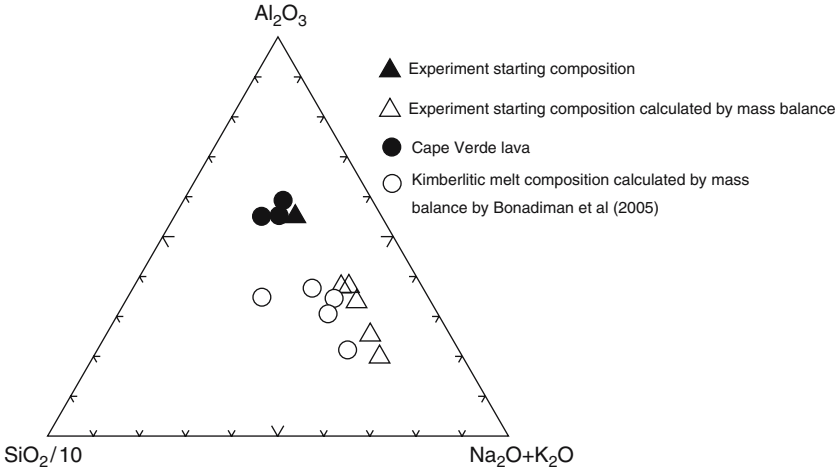

Fig. 10 Summary of the results of mass balance calculations using data from Shaw (1999) compared to the results of mass balance calculations by Bonadiman et al. (2005). *Closed triangle* shows the real composition of the solvent melt in orthopyroxene dissolution experiments. *Open triangles* show the composition of the solvent melt estimated using the linear mixing model used by Bonadiman et al (2005). Note that the calculated melt is too rich in Na and K because of the effects of uphill diffusion The kimberlitic melt calculated by Bonadiman et al. (2005) is shown as *open circles*. The composition of the Sal lavas are shown as *filled circles*. The melt composition calculated by Bonadiman et al can be explained by reaction of Cape Verde lava with xenolith minerals

Table 5 Input parameters and result of mass balance modeling (experiment op4 from Shaw 1999)

	Measured composition of phases used/produced in experiments						
	Reactants		Products			Calculated reactant melt	Calculated − actual
	Melt	opx	cpx	ol	Glass		
SiO_2	41.15	57.14	55.09	41.95	61.69	42.86	1.71
TiO_2	2.74	0.04	0.12	0.00	0.40	0.48	−2.26
Al_2O_3	12.10	2.85	0.47	0.02	9.59	6.29	−5.81
FeO	10.11	5.51	3.09	8.27	5.29	7.35	−2.76
MnO	0.18	0.14	0.05	0.19	0.11	0.12	−0.06
MgO	11.24	33.10	19.77	49.36	5.77	12.27	1.03
CaO	15.56	0.86	19.80	0.33	4.32	15.31	−0.25
Na_2O	2.76	0.09	0.52	0.02	3.47	4.43	1.67
K_2O	3.04	0.00	0.01	0.03	7.92	9.85	6.81
P_2O_5	1.02	0.00	0.00	0.00	0.05	0.06	−0.96
Total	99.90	99.73	98.92	100.17	98.61	99.02	
Observed (%)			23	42	35		
Calculated (%)			19	41	40		

observation that the zones are generally thickest on crystal surfaces near the host lava and thinnest on surfaces either protected from the lava, by being partly or completely enclosed in another mineral, or toward the center of the xenolith (Fig. 4). Also, there is a distinct association of reaction zones with veinlets of melt that are directly connected to the host lava. Deviations from this relationship can be directly related to thin veins of host lava that fill fractures in the xenolith.

Duration of reaction

A simple Stokesian approach to the derivation of xenolith immersion times, i.e. a single stage of magma ascent during which the magma ascent velocity is greater than the settling velocity of the xenoliths, yields times of a few hours for the Sal xenoliths. Recent studies however, have argued that the derivation of xenolith residence times from a Stokes' law approach to magma ascent and xenolith settling can lead to large errors (e.g. Klügel 1998; Shaw 2004; Shaw and Klügel 2002). Continuous flow of magma from source to surface does not necessarily occur and a much longer time may be available for reaction if the xenolith-bearing magma stalled in a crustal magma chamber during its journey to surface.

The immersion time of the xenoliths in the magma can be estimated from the zonation profiles in olivine if information on the temperature, oxygen fugacity and melt composition are available. The temperature of reaction is taken to be 1,175°C (see above for details). The oxygen fugacity was taken to be at the QFM buffer and the magma composition was assumed to be constant at mg# 64–67 based on the limited range of olivine rim compositions. From these assumptions, the Fe–Mg interdiffusion coefficient can be calculated from the experimental data of Chakraborty (1997) with an log (fO_2) dependence of 1/6 (Buening and Buseck 1973). Since only one surface of each grain was exposed to melt, the effects of 2-D and 3-D diffusion as described by Costa and Chakraborty (2004) may be neglected and the diffusion profiles modeled using a one-dimensional solution to the diffusion equation (see Shaw 2004 for details).

As diffusion in olivine is strongly anisotropic, the orientation information from EBSD analysis was used to determine the relation of the traverses to the a, b and c axes of each grain using the equations presented by Costa and Chakraborty (2004). Profiles for which crystallographic data were unavailable were modeled using the maximum Fe–Mg interdiffusion rate of is 9.92×10^{-5} μm/s^2.

For the profiles modeled, there are three distinct sets of timing relations:

(1) Olivine in contact with orthopyroxene reaction zones or infiltrated glass veins shows no variation in Fo in three of the four profiles. Based on the maximum diffusion rate and the spacing of points in the traverses these grains were in contact with melt for a period of less than 14 days. Modeling of the single sample that has a narrow profile, shows that it developed in ~18 days. Even in the olivines that lack evidence of Fe–Mg interdiffusion, there is a well-developed compositional variation in CaO. Klügel (1998) suggested that profiles of this type developed in olivine that was in contact either with a small volume reservoir of mafic melt or a silicic melt with high CaO. In the first case, there would have been insufficient Fe and Mg present to change the Fo content of the olivine. In the second case, the melt may have been in equilibrium with olivine in terms of Fe–Mg but not Ca.
(2) Olivine in contact with lava or with sieve-textured clinopyroxene gives reaction times from 23 days to ~4.5 years. The shorter durations likely indicate that the xenoliths were disaggregating during their residence in the magma, exposing new crystals to the

magma. This process would have been aided by complete dissolution of orthopyroxene at lava–xenolith contacts and by opening of fractures in the xenolith due to decompression The spread of data for the oriented and random traverses (Table 6) are in the same range.

(3) Olivine xenocrysts indicate immersion times of between 4 and 7 years. Most of these likely result from complete disaggregation of xenoliths. The contact times for these samples are the least reliable since the 1-D model does not take into account the fact that these grains were completely surrounded by melt. Thus, these estimates would appear to represent minimum contact times (see discussion in Costa and Chakraborty 2004).

Orthopyroxene reaction textures

As shown earlier, interaction of the silica undersaturated host magma with xenolith orthopyroxene resulted in the formation of the reaction zones. These reaction zones result from incongruent dissolution of orthopyroxene and the initial formation of a reaction zone of olivine and silica-rich melt. As the reaction zone develops, the silica-rich melt becomes enriched in alkalis due to uphill diffusion from the solvent melt. In addition, diffusion of Ca from the solvent into the reaction zone, eventually stabilizes clinopyroxene (see Shaw 1999; Shaw et al. 1998 for more details).

Disaggregation of the xenoliths could have been accomplished by the incongruent dissolution of orthopyroxene. The observation of completely reacted orthopyroxene grains at xenolith margins (Fig. 4a) supports this hypothesis. Shaw et al. (1998) and Shaw (1999) showed that orthopyroxene dissolution is very rapid and that grains the size of those in the Sal xenoliths should dissolve in around 60 days. It is clear from the petrographic observations that some of the orthopyroxenes survived much longer than this. There are three likely reasons for this. First, not all orthopyroxene grains were exposed to melt for the entire immersion period. Second, as the magma temperature decreased, the reaction rate would have decreased. Thirdly, it is possible that the presence of a reaction zone would have armoured the orthopyroxene from further reaction as has been suggested by Klügel (2001a).

Spinel reaction textures

The narrow rims of sieve texture on many of the spinels are also a result of interaction with melt. The depletion

Table 6 Calculated magma–olivine contact times

Location	Traverse#	Sample	Duration	Profile type	Orientation known?
Olivine–clinopyroxene	8	7b	2.3 years	3	No
Olivine–glass vein	11	4	< 14 days	No Fe–Mg profile	No
Olivine–glass vein	12	4	< 14 days	No Fe–Mg profile	No
Olivine–lava	3	1	1.85 years	1a	No
Olivine–lava	16	1	131 days	1a	No
Olivine–lava	1	1	140 days	1a	No
Olivine–lava	14	1	220 days	1a	No
Olivine–lava	5	1	307 days	1a	No
Olivine–lava	24	1	125 days	1a	Yes
Olivine–lava	23	1	312 days	1a	Yes
Olivine–lava	17	2	332 days	1a	No
Olivine–lava	19	3	265 days	1a	No
Olivine–lava	18	3	58 days	1a	No
Olivine–lava	21	4	1.35 years	1a	No
Olivine–lava	20	4	302 days	1a	No
Olivine–lava	9	4	72 days	1b	No
Olivine–lava	29	4	1.26 years	1a	Yes
Olivine–lava	26	4	1.87 years	1a	Yes
Olivine–lava	32	4	130 days	1a	Yes
Olivine–lava	31	4	188.5 days	1a	Yes
Olivine–lava	25	4	2.18 years	1a	Yes
Olivine–lava	28	4	215 days	1a	Yes
Olivine–lava	30	4	3.53 years	1a	Yes
Olivine–lava	27	4	97.1 days	1a	Yes
Olivine–lava	36	5	202 days	1a	Yes
Olivine–lava	33	5	243 days	1a	Yes
Olivine–lava	35	5	352 days	1a	Yes
Olivine–lava	34	5	355 days	1a	Yes
Olivine–lava	7	7	23 days	1b	No
Olivine–lava	37	7	4.4 years	1a	Yes
Olivine–opx reaction zone	10	4	18 days	1a	No
Olivine–opx reaction zone	6	5	< 14 days	No Fe–Mg profile	No
Xenocryst–lava	2	1	7.25 years	1b	No
Xenocryst–lava	15	1	4 years	4	No

of Al, and Mg and enrichment of Cr in the rims suggests that aluminum and magnesium were selectively depleted by the reaction which led to enrichment in Cr. This trend can be interpreted using the $MgO–Al_2O_3–Cr_2O_3$ phase diagram of Wilde and Rees (1943) as removal of a component with low thermal stability, leaving behind a residue with a higher thermal stability. Addition of Ti and Fe was a result of diffusion of these components into the secondary spinel from the host magma.

Clinopyroxene reaction textures

The similarity of texture between clinopyroxene and spinel suggests a similar mechanism of formation in which the fraction of the grain with the lowest thermal stability is dissolved into the melt leaving a residue that is closer to equilibrium with the melt and has higher thermal stability. Comparison of the compositional trends observed from core to rim in the sieve-textured clinopyroxene with the compositional changes induced by melting (Hirose and Kawamoto 1995) show the same general pattern as is observed in the earliest stages of partial melting, i.e. a decrease in Na and Al and increase in Ca. Thus, we interpret the sieve texture to have developed by selective removal of fusible components from the clinopyroxene leaving behind a more refractory residue. The sieve texture results from the loss of volume associated with this process.

The nature of the reaction process

The formation of sieve textured clinopyroxene and spinel appears to require the presence of a silica-rich melt. In all the grains examined in this study, the melt films and pockets are similar in composition to that formed by host melt—orthopyroxene reaction. Thus, we suggest that the formation of sieve texture requires a precursor reaction of orthopyroxene with the host melt to form the silica and alkali-enriched melt. This melt then migrates along grain boundaries where it interacts with spinel and clinopyroxene.

Conclusions

All of the secondary textures in the xenolith suite from Sal are of low pressure origin and are due to interaction with the host magma, during their residence in a crustal or upper mantle magma chamber. Modeling of the diffusion profiles in olivine indicate that the xenoliths resided the magma chamber for between approximately 3–4 years prior to their eruption at the surface. The previous interpretation of metasomatism of the mantle by ultrapotassic magma cannot be supported by this study; indeed, it is processes of uphill diffusion that occurred during reaction, particularly of orthopyroxene, that led to the high Na and K contents of the glasses.

Acknowledgments This work was funded by an NSERC Discovery grant to CSJS. Thanks to Oskar Leitner of the Bayerisches Geoinstitut for preparing the thin sections and Douglas Hall and Ryan Barr for their assistance with electron microprobe analyses. Thanks also to Alex Rocholl for his comments on an earlier version of this manuscript. We are grateful to Andreas Klügel and Dante Canil for their comprehensive and constructive reviews.

References

Bonadiman C, Beccaluva L, Coltorti M, Siena F (2005) Kimberlite-like Metasomatism and 'Garnet Signature' in spinel-peridotite xenoliths from sal, Cape Verde archipelago: relics of a sub-continental Mantle domain within the Atlantic oceanic lithosphere. J Petrol 46(12):2465–2493

Brearley M, Scarfe CM, Fujii T (1984) The petrology of ultramafic xenoliths from Summit Lake, near Prince George, British Columbia. Contrib Mineral Petrol 88:53–63

Brey GP, Köhler T (1990) Geothermobarometry in four-phase lherzolites II. New thermobarometers and practical assessment of existing thermobarometers. J Petrol 31: 1353–1378

Buening DK, Buseck PR (1973) Fe–Mg lattice diffusion in olivine. J Geophys Res 78:6852–6862

BVSP (1981) Ultramafic xenoliths in terrestrial volcanics and mantle magmatic processes, basaltic volcanism on the terrestrial planets. LPI, pp 282–310

Carpenter RL, Edgar AD, Thibault Y (2002) Origin of spongy textures in clinopyroxene and spinel from mantle xenoliths, Hessian depression, Germany. Mineral Petrol 74:149–162

Chakraborty S (1997) Rates and mechanisms of Fe–Mg interdiffusion in olivine at 980° to 1300°C. J Geophys Res 102(B6):12317–12331

Coltorti M, Beccaluva L, Bonadiman C, Salvini L, Siena F (2000a) Glasses in mantle xenoliths as geochemical indicators of metasomatic agents. Earth Planet Sci Lett 183:303–320

Coltorti M, Beccaluva L, Bonadiman C, Siena F (2000b) K-rich glasses from the oceanic mantle of Cape Verde. J Conf Abstr 5(2):316

Costa F, Chakraborty S (2004) Decadal time gaps between mafic intrusion and silicic eruption obtained from chemical zoning patterns in olivine. Earth Planet Sci Lett 227:517–530

Doucelance R, Escrig S, Moreira M, Gariepy C, Kurz MD (2003) Pb-Sr-He isotope and trace element geochemistry of the Cape Verde Archipelago. Geochim Cosmochim Acta 67:3717–3733

Ghiorso MS, Sack RO (1995) Chemical mass transfer in magmatic processes. IV. A revised and internally consistent thermodynamic model for the interpolation and extrapolation of liquid–solid equilibria in magmatic systems at elevated temperatures and pressures. Contrib Mineral Petrol 119:197–212

Hirose K, Kawamoto T (1995) Hydrous partial melting of lherzolite at 1 GPa: the effect of H2O on the genesis of basaltic magmas. Earth Planet Sci Lett 133:463–473

Ionov DA, Hofmann AW, Shimizu N (1994) Metasomatism-induced melting in mantle xenoliths from Mongolia. J Petrol 35:753–785

Kelemen PB, Dick HJB, Quick JE (1992) Formation of harzburgite by pervasive melt/rock reaction in the upper mantle. Nature 358:635–641

Klügel A (1998) Reactions between mantle xenoliths and host magma beneath La Palma (Canary Islands): constraints on magma ascent rates and crustal reservoirs. Contrib Mineral Petrol 131:237–257

Klügel A (2001a) Prolonged reactions between harzburgite xenoliths and silica-undersaturated melt: implications for dissolution and Fe–Mg interdiffusion rates of orthopyroxene. Contrib Mineral Petrol 141:1–14

Klügel A (2001b) Comment on "Silicic melts produced by reaction between peridotite and infiltrating basaltic melts: ion probe data on glasses and minerals in veined xenoliths from La Palma, Canary Islands" by Wulff-Pedersen et al. Contrib Mineral Petrol 141:1–14

Köhler TP, Brey GP (1990) Calcium exchange between olivine and clinopyroxene calibrated as a geothermobarometer for natural peridotites from 2 to 60 kb with applications. Geochim Cosmochim Acta 54:2375–2388

Liang Y, Elthon D (1990) Geochemistry and Petrology of Spinel Lherzolite Xenoliths From Xalapasco de La Joya, San Luis Potosi, Mexico: partial melting and mantle metasomatism. J Geophys Res B95:15859–15877

Morimoto N, Fabries J, Ferguson AK, Ginzburg IV, Ross M, Seifert FA, Zussman J, Aoki K, Gottardi G (1988) Nomenclature of pyroxenes. Am Mineral 73(9–10):1123–1133

de Paepe P, Klerkx J (1971) Peridotite nodules in nephelinites from Sal (Cape Verde Islands). Ann Soc Géol Belg 41:311–316

Pike JEN, Schwarzman EC (1976) Classification of textures in ultramafic xenoliths. J Geol 85:49–61

Qi Q, Taylor LA, Zhou X (1995) Petrology and geochemistry of mantle peridotite xenoliths from SE China. J Petrol 36:55–79

Ryabchikov ID, Ntaflos N, Kurat G, Kogarko LN (1995) Glass-bearing xenoliths from Cape Verde: evidence for a hot rising mantle jet. Mineral Petrol 55:217–238

Shaw CSJ (1999) Dissolution of orthopyroxene in basanitic magma between 04 and 2 GPa: further implications for the origin of Si-rich alkaline glass inclusions in mantle xenoliths. Contrib Mineral Petrol 135:114–132

Shaw CSJ (2004) The temporal evolution of three magmatic systems in the West Eifel volcanic field, Germany. J Volcanol Geothermal Res 131:213–240

Shaw CSJ, Edgar AD (1997) Post-entrainment mineral-melt reactions in spinel peridotite xenoliths from Inver, Donegal, Ireland. Geol Mag 134:771–779

Shaw CSJ, Klügel A (2002) The pressure and temperature conditions and timing of glass formation in mantle-derived xenoliths from Baarley, West Eifel, Germany: the case for amphibole breakdown, lava infiltration and mineral-melt reaction. Mineral Petrol 74:163–187

Shaw CSJ, Thibault Y, Edgar AD, Lloyd FE (1998) Mechanisms of orthopyroxene dissolution in silica-undersaturated melts at 1 atmosphere and implications for the origin of silica-rich glass in mantle xenoliths. Contrib Mineral Petrol 132:354–370

Shaw CSJ, Eyzaguirre J, Fryer BJ, Gagnon J (2005) Regional variations in the mineralogy of metasomatic assemblages in mantle xenoliths from the West Eifel Volcanic Field, Germany. J Petrol 46:945–972

Wilde WT, Rees WJ (1943) Ternary system $MgO-Al_2O_3-Cr_2O_3$. Trans Br Ceram Soc 42:123–155

Wulff-Pedersen E, Neumann E-R, Vannucci R, Botazzi P, Ottolini L (1999) Silicic melts produced by reaction between peridotite and infiltrating basaltic melts: ion probe data on glasses and minerals in veined xenoliths from La Palma, Canary Islands. Contrib Mineral Petrol 137:59–82